

CMOS compatible reconfigurable filter for high bandwidth non-blocking operation

Hugo L. R. Lira,¹ Carl B. Poitras,¹ and Michal Lipson^{1,2,*}

¹*School of Electrical and Computer Engineering, Cornell University, Ithaca, N.Y. 14853, USA*

²*Kavli Institute at Cornell for Nanoscale Science, Cornell University, Ithaca, N.Y. 14853, USA*

[*ml292@cornell.edu](mailto:ml292@cornell.edu)

Abstract: We design, fabricate and characterize a CMOS-compatible, Mach-Zehnder-coupled, second-order-microring-resonator filter with large Free Spectral Range and demonstrate non-blocking thermo-optical filter reconfiguration. The device consists of 10- μm radius silicon microring resonators, with an FSR equivalent to that of a structure consisting of 5- μm radii microrings. The structure is reconfigurable over an 8.5 nm range without blocking other channels in the network.

© 2011 Optical Society of America

OCIS codes: (130.3120) Integrated optics devices; (130.4815) Optical switching devices.

References and links

1. J. Palais, *Fiber Optic Communications* (Prentice Hall, 1988).
2. D. A. B. Miller and H. M. Ozaktas, "Limit to the bit-rate capacity of electrical interconnects from the aspect ratio of the system architecture," *J. Parallel Distrib. Comput.* **41**, 42-52 (1997).
3. N. Magen, A. Kolodny, U. Weiser, and N. Shamir, "Interconnect-power dissipation in a microprocessor," in *Proceedings of the 2004 International Workshop on System Level Interconnect Prediction* (ACM, 2004), pp. 7-13.
4. A. Shacham, K. Bergman, and L. P. Carloni, "Photonic networks-on-chip for future generations of chip multi-processors," *IEEE Trans. Comput.* **57**, 1246-1260 (2008).
5. C. Batten, A. Joshi, J. Orcutt, A. Khilo, B. Moss, C. W. Holzwarth, M. A. Popovic, H. Q. Li, H. I. Smith, J. L. Hoyt, F. X. Kartner, R. J. Ram, V. Stojanovic, and K. Asanovic, "Building Many-Core Processor-to-DRAM Networks with Monolithic CMOS Silicon Photonics," *IEEE Micro* **29**, 8-21 (2009).
6. Y. Goebuchi, T. Kato, and Y. Kokubun, "Fast and stable wavelength-selective switch using double-series coupled dielectric microring resonator," *IEEE Photonics Technol. Lett.* **18**, 538-540 (2006).
7. Q. Xu, D. Fattal, and R. G. Beausoleil, "Silicon microring resonators with 1.5- μm radius," *Opt. Express* **16**, 4309-4315 (2008).
8. S. Xiao, M. H. Khan, H. Shen, and M. Qi, "A highly compact third-order silicon microring add-drop filter with a very large free spectral range, a flat passband and a low delay dispersion," *Opt. Express* **15**, 14765-14771 (2007).
9. M. S. Nawrocka, T. Liu, X. Wang, and R. R. Panepucci, "Tunable silicon microring resonator with wide free spectral range," *Appl. Phys. Lett.* **89**, 071110-071113 (2006).
10. K. Oda, N. Takato, and H. Toba, "A wide-FSR wave-guide double-ring resonator for optical FDM transmission-systems," *J. Lightwave Technol.* **9**, 728-736 (1991).
11. G. Barbarossa and A. Matteo, "Novel double-ring optical-guided-wave Vernier resonator," *IEE Proc.-Optoelectron.* **144**, 203-208 (1997).
12. M. R. Watts, T. Barwicz, M. A. Popovic, P. T. Rakich, L. Socci, E. P. Ippen, H. I. Smith, and F. Kaertner, "Microring-Resonator Filter with Doubled Free-Spectral-Range by Two-Point Coupling," in *Conference on Lasers and Electro-Optics/Quantum Electronics and Laser Science and Photonic Applications Systems Technologies*, Technical Digest (CD) (Optical Society of America, 2005), paper CMP3.
13. W. Green, R. Lee, G. DeRose, A. Scherer, and A. Yariv, "Hybrid InGaAsP-InP Mach-Zehnder racetrack resonator for thermo-optic switching and coupling control," *Opt. Express* **13**, 1651-1659 (2005).
14. L. Zhou and A. W. Poon, "Electrically reconfigurable silicon microring resonator-based filter with waveguide coupled feedback," *Opt. Express* **15**, 9194-9204 (2007).

15. L. Chen, N. Sherwood-Droz, and M. Lipson, "Compact bandwidth-tunable microring resonators," *Opt. Lett.* **32**, 3361-3363 (2007).
16. H. L. Lira, M. Lipson, and C. B. Poitras, "Non-Blocking Operation of a Tunable Compact Optical Filter with Large FSR," in *CLEO:2011 - Laser Applications to Photonic Applications*, OSA Technical Digest (CD) (Optical Society of America, 2011), paper CTuN3.
17. B. Little, S. Chu, H. Haus, J. Foresi, and J. Laine, "Microring resonator channel dropping filters," *J. Lightwave Technol.* **15**, 998-1005 (1997).
18. A. Melloni and M. Martinelli, "Synthesis of direct-coupled-resonators bandpass filters for WDM systems," *J. Lightwave Technol.* **20**, 296-303 (2002).
19. R. Orta, P. Savi, R. Tascone, and D. Trinchero, "Synthesis of multiple-ring-resonator filters for optical systems," *IEEE Photonics Technol. Lett.* **7**, 1447-1449 (1995).
20. H. L. R. Lira, S. Manipatruni, and M. Lipson, "Broadband hitless silicon electro-optic switch for on-chip optical networks," *Opt. Express* **17**, 22271-22280 (2009).
21. G. Cocorullo and I. Rendina, "Thermo-optical modulation at 1.5 μm in silicon etalon," *Electron. Lett.* **28**, 83-85 (1992).

1. Introduction

State-of-the-art multi-core microprocessor systems have already achieved astonishing performances, but the tradeoff between signal attenuation and bandwidth in metallic wires compromises further progress [1, 2, 3]. A compelling alternative to decouple loss and bandwidth relies on Optical Networks-on-Chip (ONoC), which opens new possibilities to network architectures with unprecedented communication bandwidth [4, 5].

Free Spectral Range (FSR) and reconfiguration dynamics of individual filters are two pivotal points which set boundaries to the overall capacity of an ONoC. Both are important for most metrics involving networks efficiency, being crucial factors on the overall aggregate bandwidth and network latency, respectively. The aggregate bandwidth of an ONoC is limited by the sum of the bandwidths of all channels comprising the network, which is ultimately limited by the FSR of individual channels. And a reconfigurable network might suffer unnecessary latency if single channel reallocation requires disabling other channels.

Here, by the proper operation of a Mach-Zehnder interferometer (MZI) enhanced second-order microring-resonator filter, we demonstrate a non-blocking – or hitless [6] – reconfigurable filter with large FSR. The ability to efficiently increase the number of channels in a network has been demonstrated in passive non-reconfigurable structures, in a variety of ways, for example, by using small microring resonators [7, 8, 9], Vernier filters [10, 11], and by merging MZI's with microring resonators (Fig. 1a) [11, 12, 13, 14, 15]. The last approach is chosen for this work because it has the interesting features of doubling the FSR without imparting high radiation losses (intrinsic to tight bends) and without the typical insertion loss for misaligned resonances (intrinsic to Vernier filters). This paper expands our work presented in [16], presenting a detailed description of the synthesis procedure and non-blocking operation.

2. Description, synthesis and non-blocking operation

The device, shown in Fig. 1a, consists of a modified second-order microring-resonator filter, where the coupling between the microring and the waveguide is MZI assisted with a two-point coupling topology instead of the usual single-point coupling (red inset in Fig. 1b). The MZI is composed of 2 arms with lengths L_{mz} and L_{mzr} , with equal field coupling κ for both coupling regions, as shown in Fig. 1a. The MZI provides a periodic wavelength dependency for the coupling between bus waveguides and resonators, with periodicity set by the arm length difference $\Delta L = L_{mz} - L_{mzr}$. In Fig. 1b, the spectral responses of the ring and of the MZI are shown in red and green, respectively. For a given relation between the values of ΔL and κ one can achieve the removal of every other resonance of the microring leading to a doubled FSR filter with a box-like transfer function, as shown in Fig. 1c.

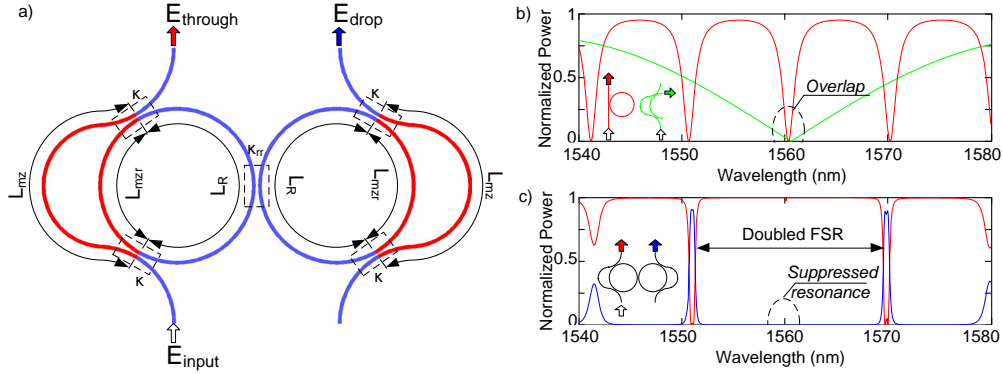


Fig. 1. (a) Schematics of a second-order filter with MZ arms. (b) Transfer function of a microring resonator (red) and effective coupling κ_{eff} of a MZI (green). (c) Transfer function of through (red) and drop (blue) ports of the filter.

In order to determine the required values of ΔL and κ , one needs to ensure that the minimum coupling κ_{eff} of the MZI overlaps with the resonance to be suppressed. The coupling (κ_{eff}) and transmission (t_{eff}) coefficients of an MZI are extracted from the input to output transfer function

$$\begin{pmatrix} E_{out1} \\ E_{out2} \end{pmatrix} = \exp\left(i\frac{2\pi}{\lambda}n_{eff}(\lambda, T)\frac{L_{mz}+L_{mzr}}{2}\right) \cdot \begin{pmatrix} t_{eff} & i \cdot \kappa_{eff} \\ i \cdot \kappa_{eff} & \bar{t}_{eff} \end{pmatrix} \begin{pmatrix} E_{in1} \\ E_{in2} \end{pmatrix} \quad (1)$$

with

$$\kappa_{eff}(\lambda, T) = 2\kappa t \cos\left(\frac{2\pi}{\lambda}n_{eff}(\lambda, T)\frac{\Delta L}{2}\right) \quad (2)$$

$$t_{eff}(\lambda, T) = 2t^2 \cos\left(\frac{2\pi}{\lambda}n_{eff}(\lambda, T)\frac{\Delta L}{2}\right) - \exp\left(-i\frac{2\pi}{\lambda}n_{eff}(\lambda, T)\frac{\Delta L}{2}\right) \quad (3)$$

where n_{eff} is the effective refractive index of the waveguides comprising the MZI, which is a function of wavelength λ and temperature T . and \bar{t}_{eff} is the complex conjugate of t_{eff} . Therefore, the minimum coupling at the wavelength λ_0 is obtained when $\kappa(\lambda_0) = 0$, which leads to:

$$\Delta L(m_2) = \frac{\lambda_{m_1}}{n_{eff}(\lambda_{m_1})} \cdot \left(m_2 - \frac{1}{2}\right), m_2 \in \mathbb{N}^* \quad (4)$$

where the wavelength λ_{m_1} is obtained from the resonance condition of a microring:

$$2\pi R n_{eff}(\lambda_{m_1}) = m_1 \lambda_{m_1}, m_1 \in \mathbb{N}^* \quad (5)$$

Where R is the radius of the microring. Combining Eq. 2 and Eq. 5, the equation for the effective coupling at λ_{m_1-1} :

$$\kappa_{eff}(\lambda_{m_1-1}) = 2\kappa t \cos\left[\frac{m_1-1}{2m_1}(1+2m_2)\pi\right] \quad (6)$$

Therefore the coupling κ is given by:

$$\kappa(m_2) = \sqrt{\frac{1}{2} - \frac{1}{2} \sqrt{1 - \kappa_{eff}^2(\lambda_{m_1-1}) \left[\sin\left(\frac{1+2m_2}{2m_1}\pi\right)\right]^{-2}}} \quad (7)$$

In order to obtain real solutions, minimum and maximum boundaries are set for the possible values of m_2 :

$$\frac{m_1}{\pi} \operatorname{asin} [k_{eff}(\lambda_{m_1-1})] - \frac{1}{2} \leq m_2 \leq \frac{m_1}{\pi} \{ \pi - \operatorname{asin} [k_{eff}(\lambda_{m_1-1})] \} - \frac{1}{2} \quad (8)$$

The geometry of the device is determined by choosing values for m_1 and m_2 that obey Eq. 8, which are then used to calculate ΔL and κ using Eqs. 4 and 7, while the bandwidth and passband ripple of the box-like filter are determined by the effective coupling $\kappa_{eff}(\lambda_{m_1-1})$ and ring to ring coupling κ_{rr} , which are obtained from filter synthesis methods [17, 18, 19, 20]. For example, Fig. 2 shows a few possibilities of transfer functions for different values of m_1 and m_2 and fixed values of $\kappa_{eff}(\lambda_{m_1-1})$ and κ_{rr} . The examples shown in Figs. 2a, b, and c are for $m_2 = (m_1 - 1)/2$, $m_2 = (m_1 - 1)/3$, and $m_2 = (m_1 - 1)/5$, which result in $\Delta L = 2\pi R/2$, $\Delta L \approx 2\pi R/3$, and $\Delta L \approx 2\pi R/5$, respectively, all of them with 60 GHz flatband bandwidth and -20 dB passband ripple at resonance. All figures show a doubled FSR around the suppressed resonance at λ_{m_1} , with a box-like resonance at the next resonance at λ_{m_1-1} and distinct behavior for further resonances, depending on the coupling provided by the MZI for each of them. In Fig. 2a, every other resonance is removed, while in Fig. 2b one out of every three resonances is removed, and in Fig. 2c one out of every five resonances is removed. We observe that the coupling, shown in green, has a sinusoidal behavior. Changing its periodicity and amplitude directly effects the sensitivity around the resonances λ_{m_1} and λ_{m_1-1} . Consequently, the coupling is more (less) sensitive around the resonance λ_{m_1-1} (λ_{m_1}) for smaller m_2 values, which can be an important criteria when choosing the design parameters for specific applications.

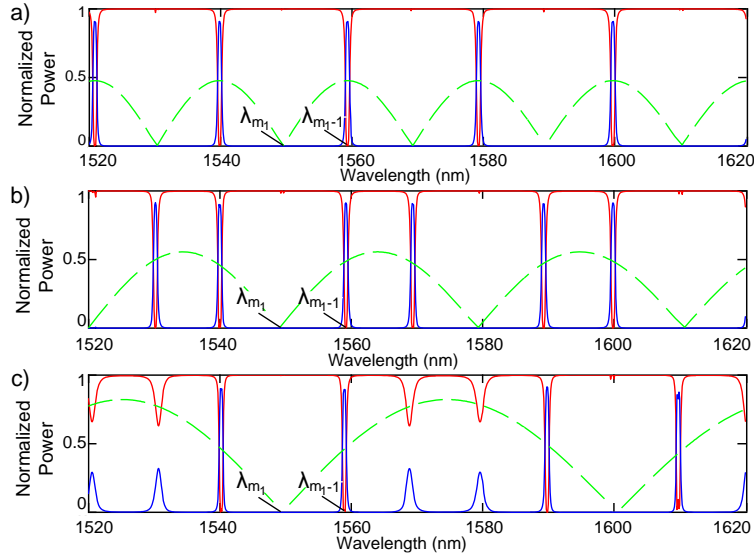


Fig. 2. Examples of possible transfer function. In red we have the through port, the drop port is in blue, and, in green, we have the wavelength dependency of the effective coupling κ_{eff} for (a) $m_2 = (m_1 - 1)/2$, (b) $m_2 = (m_1 - 1)/3$, and (c) $m_2 = (m_1 - 1)/5$. All simulations considered 10 μm radius silicon microrings, surrounded by SiO_2 , with 6 dB/cm propagation losses.

In order to obtain non-blocking operation of the filter, the following sequence of 3 events is implemented: the refractive index of the microring and of the MZI at the right is modified, which changes the box-like filter into an all-pass filter; the refractive index of the entire structure

is modified altogether, moving the all-pass filter to a new wavelength; and finally the excess change in the refractive index of the microring and MZI at the right is removed, so that the all-pass filter transitions back to a box-like filter at a new wavelength. We make use of the strong thermo-optical effect present in silicon to change the refractive index and achieve non-blocking tuning [21].

Figure 3 shows the transmission response of the structure and its non-blocking nature following the three steps of temperature tuning outlined above. The through port and drop port transmissions (E_t and E_d , respectively) were plotted using

$$E_t = \frac{t_{Left} - at_{Left}t_{rr}\overline{t_{Right}}\phi_{Right} - at_{rr}\phi_{Left} + a^2\overline{t_{Right}}\phi_{Right}\phi_{Left}}{1 - a(\phi_{Left}\overline{t_{Left}} + \phi_{Right}\overline{t_{Right}})}t_{rr} + a^2\phi_{Left}\overline{t_{Left}}\phi_{Right}\overline{t_{Right}}}\phi_1 E_i \quad (9)$$

$$E_d = \frac{-ia\kappa_{Left}\kappa_{rr}\kappa_{Right}\sqrt{\phi_{Left}\phi_{Right}}}{1 - a(\overline{t_{Left}}\phi_{Left} + \overline{t_{Right}}\phi_{Right})}t_{rr} + a^2\overline{t_{Left}}\phi_{Left}\overline{t_{Right}}\phi_{Right}}\sqrt{\phi_1\phi_2}E_i \quad (10)$$

where

$$\phi_{Left/Right} = \exp\left[i\frac{2\pi}{\lambda}n_{eff}(T_{Left/Right})\left(2\pi R + \frac{\Delta L}{2}\right)\right] \quad (11)$$

$$\phi_{1/2} = \exp\left(i\frac{2\pi}{\lambda}n_{eff}(T_{Left/Right})\frac{L_{mz} + L_{mzr}}{2}\right) \quad (12)$$

$$a = \exp[-\alpha(\pi R + \Delta L)] \quad (13)$$

where $t_{Left} = t_{eff}(T_{Left})$, $\kappa_{Left} = \kappa_{eff}(T_{Left})$, $\overline{t_{Left}}$ is the complex conjugate of t_{Left} , $t_{Right} = t_{eff}(T_{Right})$, and $\kappa_{Right} = \kappa_{eff}(T_{Right})$, $\overline{t_{Right}}$ is the complex conjugate of t_{Right} , and α is the propagation loss. T_{Left} is the temperature of the left microring and of the Mach-Zehnder arm connected to it, and T_{Right} is the temperature of the right microring and of the Mach-Zehnder arm connected to it. Figure 3(i) shows the transmission when $T_{Left} = T_{Right} = T_0$. Figure 3(ii) shows the transfer function when the temperature of right ring and MZI is increased to $T_{Right} = T_1$, obtaining an all-pass filter. Figure 3(iii) shows the transfer function when the temperature of the full device is increased by T_F so that $T_{Right} = T_1 + T_F$ and $T_{Left} = T_F$, shifting the all-pass filter to a new location. Finally, Figure 3(iv) shows the transfer function when temperature of the right side of the device is reduced to T_F , reallocating the box-like transfer function at a new wavelength. Even though it is clear in Fig. 3 that the reconfiguration process does not block other channels, we observe that it imparts about 1 dB insertion loss to the intermediate wavelengths. Optimization of design parameters can be used to reduce even more such reconfiguration insertion loss.

3. Fabrication, experiment and results

We fabricated the structure using a CMOS-compatible process. As shown in Fig. 4a, doped Si heaters were formed inside the microrings and in the surroundings of the external arms of the MZI's, with doping level of $1 \times 10^{20} \text{ cm}^{-3}$, using Ar^- as a dopant. The cross section of the heaters is 215 nm high by 1000 nm wide, while the cross section of the crystalline silicon waveguides is 215 nm high by 450 nm wide. Heaters in inner part of bends are placed 1 μm from the waveguides, while heaters in outer part of bends are placed 2 μm from the waveguides, as can be seen in Fig. 4a. A thin 35 nm silicon slab is left underneath the structure to enhance the heat transfer from the heaters to the waveguides. The slab is removed elsewhere mainly to improve the coupling from the optical fiber to the inverse taper used as input of the device. Since Fig. 4a is slightly angled, scale and dimensions of the device are better verified in Fig. 4b. The overall structure is fabricated on an SOI wafer with a 3 μm buried oxide and is clad with

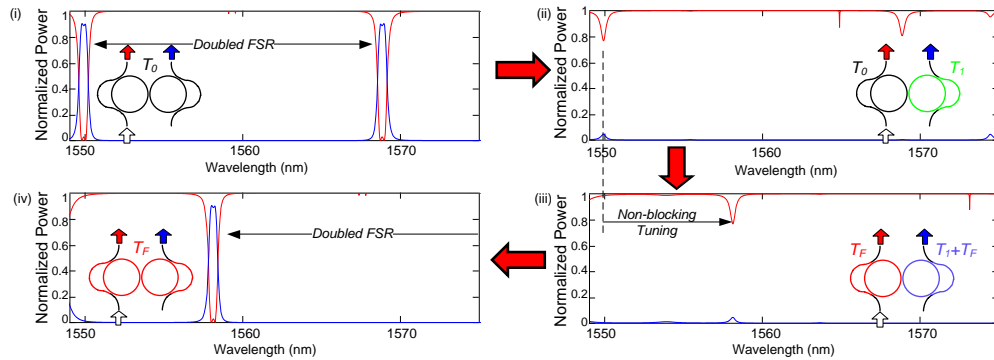


Fig. 3. Non-blocking tuning. (i) Initial transfer function of the filter, with the whole structure at the same temperature T_0 . (ii) All-pass transfer function after the right side of the filter is at temperature T_1 . (iii) The all-pass transfer function is shifted completely by increasing the temperature of the whole structure by T_F . (iv) Final transfer function, obtained by reducing the temperature of the right side down to T_F .

a 1.2 μm of SiO_2 . Vias are etched for electrical contacts, where a thin stack of TiSi and TiN is formed prior to the evaporation of the Cu wirings and pads. The final structure is shown in Fig. 4b.

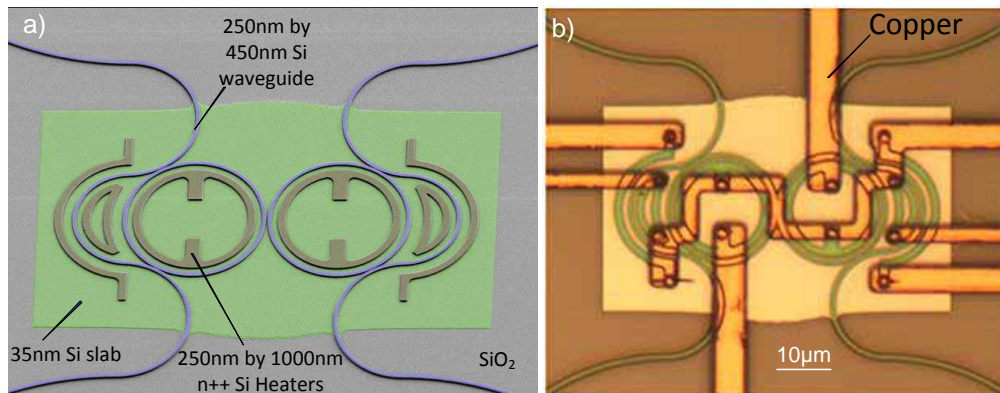


Fig. 4. (a) False-color Scanning Electron Microscope picture of the device. The waveguides are shown in blue, heaters in brown and a thin silicon slab underneath the structure is shown in green (no metal contacts shown). (b) Optical microscope picture of the final structure, with copper wiring connected through round vias to the heaters.

The transfer function of the fabricated device is measured as shown in Fig. 5a, where a doubled FSR of 19.2 nm can be observed for the 10 μm radius microrings, with its main resonance at 1594.6 nm. We observe less than 1 dB insertion loss for the drop port and 20 dB suppression for the removed resonance. The residual power dropped at the suppressed resonance (at 1604.2 nm) is about 16 dB below the signal level. This transfer function is equivalent to the one presented at Fig. 2c, with a small mismatch in the length of the MZI leading the box-like filter around 1613 nm to be slightly overcoupled. In Figs. 5b and 5c we demonstrate the non-blocking tuning of the fabricated filter. For the first step of the non-blocking tuning, we apply 28 mW to the heater inside the microring connected to the drop port and to the Mach-Zehnder arm connected to it, which changes the box-like transfer function (Fig. 5a) to an all pass transfer

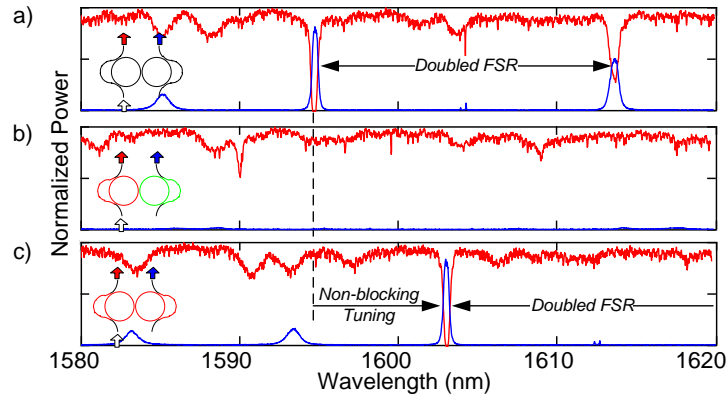


Fig. 5. (a) Original spectrum of the device, with through (red) and drop (blue) ports presenting the doubled FSR. (b) Spectrum after changing the effective index of the cavity coupled to the drop port. No resonances are observed. (c) New resonance of the filter after non-blocking tuning.

function (Fig. 5b), as expected. In Fig. 5c we show the final step of the tuning, where a new central resonance wavelength, at 1603.1 nm, is observed under 115 mW of heat power applied for all heaters. The thermal response of the heaters was measured to be in the order of 10 μ s. Non-blocking operation is clear from the experimental results, confirming that a doubled FSR filter can be reconfigured from a wavelength to another with negligible insertion loss for intermediate wavelengths.

4. Conclusion

We fabricate and characterize a CMOS-compatible, Mach-Zehnder-coupled, second-order-microring-resonator filter with doubled free spectral range and demonstrate non-blocking thermo-optical filter reconfiguration. We demonstrate that non-blocking tuning can be achieved for a doubled FSR filter, which translates to a higher throughput for NoC's. It is important to note that in the current configuration, when the device is reconfigured and the refractive index of part of the structure is modified to achieve the all-pass filter, an overcoupled resonance is obtained, which still has a small power penalty and imparts some loss (< 1 dB) on other channels allocated between the initial and final wavelength. Even though the procedure described does not block the communication of other channels, its power penalty must be considered in the network design, and may limit the number of channels that can be reconfigured simultaneously.

Acknowledgments

This work was performed in part at the Cornell NanoScale Facility, a member of the National Nanotechnology Infrastructure Network, which is supported by the National Science Foundation. This work was partly supported by the NSF award #ECCS-0903406. Hugo Lira thanks his sponsorship support provided by the Brazilian Defense Ministry.